December 1985 LRP 266/85

AXISYMMETRIC STABILITY OF HIGHLY-ELONGATED TOKAMAK PLASMA - A NEW METHOD AND INITIAL RESULTS

F. Hofmann, F.B. Marcus and A.D. Turnbull

AXISYMMETRIC STABILITY OF HIGHLY-ELONGATED TOKAMAK PLASMA - A NEW METHOD AND INITIAL RESULTS

F. Hofmann, F.B. Marcus, A.D. Turnbull

Centre de Recherches en Physique des Plasmas
Association Euratom - Confédération Suisse
Ecole Polytechnique Fédérale de Lausanne
21, Av. des Bains, CH-1007 Lausanne, Switzerland

Abstract

A new method is presented for computing global axisymmetric instabilities of tokamak plasmas in a conducting shell. The method uses a free-boundary equilibrium code to find displacement vectors compatible with ideal MHD. It is applied to the computation of vertical instability growth rates of highly-elongated, race-track shaped plasmas. Results obtained for up-down symmetric configurations are compared with ERATO calculations. The effects of plasma-wall distance, plasma pressure and current profile are analyzed. In addition, the gain in stability produced by asymmetric positioning of a given plasma in a given shell is evaluated.

1. INTRODUCTION

The stabilization of axisymmetric modes in tokamak plasma is becoming an increasingly important problem in view of recent evidence that non-circular cross-sections may offer a decisive advantage with respect to the beta limit (TROYON et al., 1984; SYKES et al., 1983; STAMBAUGH et al., 1984; OKABAYASHI et al., 1984). The usual scheme for stabilizing these modes consists of passive and active elements, to deal with the fast and slow motions, respectively. The theory of passive stabilization on the fast (Alfvén) time scale has been investigated by many authors (JOHNSON et al., 1976; BERGER et al., 1977; BOBBIO et al., 1983; HAAS et al., 1975; DOBROTT et al., 1981; GOEDBLOED et al., 1972). There are basically two approaches: The first approach (JOHNSON et al., 1976 and BERGER et al., 1977) consists of solving the problem rigorously by computing all axisymmetric modes, using an ideal MHD stability code (such as PEST, ERATO). This can be a time-consuming exercise, however, especially when many different configurations must be analyzed. The second approach tries to obtain an approximate solution by using a simplified plasma model. One of the methods in this class (BOBBIO et al., 1983) consists of decomposing the plasma in a number of discrete current loops, and computing the work done by the $\vec{j} \times \vec{B}$ forces, for an assumed displacement vector. This method may give accurate results if the true mode structure happens to be similar to the assumed one. It is known, however, that axisymmetric modes in highly-elongated or bean-shaped plasmas may have a very complicated structure.

In this paper, we propose an alternate method which combines the accuracy of the first approach with the simplicity of the second.

2. THEORY

2.1 Initial Equilibrium

Any stability analysis requires an accurate equilibrium solution as a starting point. We use the FBT code (HOFMANN and JOYE, 1983) to generate free-boundary axisymmetric equilibria. FBT exists in several versions. The version which is used here has a built-in dipole and quadrupole feedback for stabilizing the outer loop iterations. This stabilization is necessary for obtaining a converged solution whenever the vertical elongation of the plasma cross-section is beyond a certain critical value ($b/a \approx 2$). The feedback is applied in the following way: At the beginning of the calculation, initial estimates of all poloidal field coil currents are specified. These estimates are usually obtained from a separate calculation (HOFMANN and MARCUS, 1984). In addition, four limiter points are assumed. The code then maintains the values of the flux function at the four limiter points equal to each other, and assumes that the corresponding flux surface defines the plasma surface. This is achieved by varying the total plasma current and by superimposing two sets of correction currents onto the poloidal field coil currents, at each step of the iteration. One of these sets of currents produces a pure radial field, and the other produces a quadrupole field. The converged solution then has $\Psi = \Psi_{lim}$ at the four limiter points.

The source functions which we will be using in this study are given by

$$\begin{aligned} p' &= c_p(\Phi + \ell\Phi^2) \\ TT' &= c_T(\Phi + \ell\Phi^2) \end{aligned} \tag{1}$$

where p is the plasma pressure, $T = RB_\phi$, $\Phi = (\Psi - \Psi_{lim})/(\Psi_{axis} - \Psi_{lim})$, c_p and c_T are constants and $c_T/c_p = R_o^2\mu_o((1/\beta)-1)$. The parameter ℓ defines the width of the current profile and β is related to the poloidal beta, $\beta_{pol} = 8\pi\int\int p\, ds/\mu_o I^2$.

2.2 Displaced Equilibrium

Let us first consider an arbitrary displacement (Fig. 1). The limiter points are shifted vertically or horizontally (H_1, H_2, H_3, H_4) and the equilibrium parameters β, ℓ and B_o are changed by small amounts, $\Delta\beta$, $\Delta\ell$ and ΔB_o. The displacement may be described by a vector $\vec{H}$, defined as

$$\vec{H} = \begin{bmatrix} H_1 \\ H_2 \\ H_3 \\ H_4 \\ \Delta\beta \\ \Delta\ell \\ \Delta B_o \end{bmatrix}$$

where B_o is the toroidal vacuum field at $R = R_o$.

In principle, we wish to compute the displaced equilibrium without changing the flux function on the shell, since the latter is assumed to be perfectly conducting. For an arbitrary displacement, this is, of course, impossible. However, the displaced equilibrium can be computed if we add a perturbation to the flux on the boundary,

$$\Delta\Psi = W + D\,Z + Q(Z^2 + R^2(0.5 - \log(\frac{R}{R_o}))) \qquad (2)$$

and if we change the plasma current by an amount ΔI_p. This gives us the four independent variables $(W,D,Q,\Delta I_p)$ which are necessary to fit the four new limiter points. The perturbation (eq. 2) contains a constant term (W), a dipole field (D) and a quadrupole field (Q). Although the perturbation is only imposed on the boundary, eq. (2), is also valid inside the shell, since it is an analytic solution of the currentless Grad-Shafranov equation, $\partial^2\Psi/\partial Z^2 + R[(\partial/\partial R)\{(1/R)(\partial\Psi/\partial R)\}] = 0$. It should be noted, however, that inside the shell, the perturbation of the flux function contains three terms, i.e. $\Delta\Psi$ as given in eq. (2), $\Delta\Psi_p$ due to the redistribution of the plasma current and $\Delta\Psi_i$ due to image currents in the shell. The dipole term in eq. (2) produces a pure radial field, whereas the quadrupole is chosen in such a way that the field null appears at $R = R_o$, $Z = 0$.

Apart from the change in the limiter position (H_1, H_2, H_3, H_4) the displaced equilibrium also uses new parameters β', ℓ', and B_o'. Those are obtained from the original ones by applying the corrections specified in the displacement vector, $\vec{H}$:

$$\begin{aligned} \beta' &= \beta + \Delta\beta \\ \ell' &= \ell + \Delta\ell \\ B_o' &= B_o + \Delta B_o \end{aligned} \qquad (3)$$

Note that a change in B_o implies induced poloidal currents in the shell and a change in ℓ represents a modification of the plasma current distribution. We assume that toroidal as well as poloidal image currents can flow freely in the conducting shell, but that no currents are induced on the plasma surface.

2.3 Ideal MHD Constraints

We now wish to select those displacements which satisfy the conservation laws of ideal MHD. For this purpose, we define a vector $\vec{T}$,

$$\vec{T} = \begin{bmatrix} \Delta\Phi_v \\ \Delta\Phi_p \\ W \\ \Delta\Psi_{axis} \\ \Delta S \\ Q \\ D \end{bmatrix}$$

where $\Delta\Phi_v$ and $\Delta\Phi_p$ are the toroidal flux changes in vacuum and plasma, respectively, W and $\Delta\Psi_{axis}$ are the corresponding poloidal flux changes, ΔS is the change in entropy and the remaining quantities are defined in eq. (2).

For small displacements, $\vec{T}$ is a linear function of $\vec{H}$,

$$\vec{T} = A\,\vec{H} \tag{4}$$

The elements of the matrix A can be found by imposing particular displacements, for example

$$\vec{H}_1 = \begin{bmatrix} H_1 \\ 0 \\ 0 \\ 0 \\ 0 \\ 0 \\ 0 \end{bmatrix}, \qquad \vec{H}_2 = \begin{bmatrix} 0 \\ H_2 \\ 0 \\ 0 \\ 0 \\ 0 \\ 0 \end{bmatrix}, \qquad \vec{H}_3 = \begin{bmatrix} 0 \\ 0 \\ H_3 \\ 0 \\ 0 \\ 0 \\ 0 \end{bmatrix}, \quad \text{etc.}$$

and computing the corresponding $\vec{T}$ vectors.

We have tested the validity of eq. (4) by computing $\vec{T}$ vectors for a large number of arbitrary displacements $\vec{H}$. We find that if the maximum surface displacement is less than about 1/50 of the minimum plasma-wall distance, then the deviations from linearity are less than ~ 1%. Under these conditions, the elements of the matrix A are independent of the assumed $\vec{H}$.

Clearly, if $\vec{T} = 0$, the constraints imposed by ideal MHD are globally satisfied and the flux on the conducting shell has been left unchanged ($\Delta\Psi = 0$). This is a special case, however, which corresponds to a state of marginal stability, as will be shown below. In general,

we cannot impose $\vec{T} = 0$ and obtain a nontrivial solution for $\vec{H}$ from eq. (4). At least one of the elements in $\vec{T}$ must be assumed nonzero. If we insist on satisfying ideal MHD constraints, there are only two possibilities, i.e. $D \neq 0$ or $Q \neq 0$. If we choose $D \neq 0$, $Q = 0$, we obtain a predominantly vertical displacement, since the boundary flux is perturbed by a pure radial field. This mode leaves the q-profile practically unchanged. If, on the other hand, we assume $Q \neq 0$, $D = 0$, we obtain a droplet-ellipse deformation which drastically changes the q-profile. This mode may be important in resistive MHD, but it is excluded in ideal MHD. Consequently, we assume $D \neq 0$, $Q = 0$, and we define a vector $\vec{T}_c$,

$$\vec{T}_c = \begin{bmatrix} 0 \\ 0 \\ 0 \\ 0 \\ 0 \\ 0 \\ D \end{bmatrix}$$

The displacement vector is then given by

$$\vec{H} = A^{-1}\vec{T}_c \qquad (5)$$

2.4 Growth Rate of the Vertical Instability

A rough estimate of the vertical growth rate can be obtained from

$$\omega^2 = \frac{2\pi\ R\ I_p\ B_R}{M\ \overline{H}} \tag{6}$$

where B_R is the radial field given by $B_R = D/R$, M is the total mass of the plasma and $\overline{H}$ is an average vertical displacement. We assume

$$\overline{H} = 0.25\ (H_1 + H_2 + 2H_0) \tag{7}$$

where H_0 is the vertical displacement of the magnetic axis and H_1 and H_2 are defined in Fig. 1. This procedure gives only a rough approximation, because we are not dealing with a rigid displacement. However, the marginal point ($B_R = 0$) is uniquely determined and its parameters do not depend on the approximation used for computing the average displacement (eq. 7).

From a practical point of view, only the marginal point is important. The exact values of the growth rates are irrelevant, since they are in any case much faster than typical decay rates of image currents in tokamak vacuum vessels.

3. RESULTS

3.1 Comparison with ERATO

In order to compare our results with ERATO calculations (GRUBER et al., 1981), we first consider up-down symmetric configurations. Let us assume an elongated equilibrium with b/a = 3, in a conducting shell with rectangular cross-section (Fig. 2). Note that all linear dimensions (a, b, a_w, b_w) are given in meters. We compute the growth rate of the vertical instability by the method outlined above as a function of the width (a_w) and height (b_w) of the shell. We then compute the same growth rates, using the ERATO stability code (GRUBER et al., 1981). In comparing the results of the two calculations (Fig. 3), we see that the marginal points ($\Omega^2 = 0$) agree almost exactly. In addition, there is surprisingly good agreement in the values of the growth rates, considering the rough approximation made in FBT. Figure 4 shows the ratio between the vertical displacements on axis (H_0) and on the top edge (H_1) as a function of the height and width of the shell. Again, we observe that, close to the marginal point, there is good agreement between ERATO and FBT results. However, as soon as we move away from the marginal point, the results disagree. This is, of course, a consequence of the fictitious radial field, $\Delta\Psi = DZ$, which is added in the FBT calculation in order to maintain the displaced plasma in equilibrium.

3.2 Pressure Effects

The effect of plasma pressure on the growth rate of the vertical instability can be seen in Fig. 5, where we show the result of a

threefold increase in β_{pol}. The external coil currents were readjusted, such that the plasma shape was unaffected by the change in β_{pol}. We note that the pressure has very little effect on the growth rates of the modes considered here.

3.3 Current Profile Effects

When the plasma current profile becomes peaked, the vertical instability growth rates increase rapidly, as can be seen in Fig. 6. Results are shown as a function of the shell width (a_w) for three different current profiles and for a shell height of b_w = 0.58 m. It is seen that a stable equilibrium, which is quite far from the marginal point, such as the one with a_w = 0.24 and ℓ = -0.5 in Fig. 6, can be driven unstable by changing the width of the current profile by only 5%.

3.4 Asymmetric Configurations

The results presented in the previous sections were obtained for up-down symmetric configurations. Assymetric configurations may also be of interest, for example during the early phases of a discharge, when the plasma height is much less than the height of the shell. Such a case is shown in Fig. 7. Starting from a symmetric configuration (a = 0.18 m, b = 0.54 m, a_w = 0.24 m, b_w = 0.90 m), the plasma is shifted upward until it comes close to the top wall. For each of the equilibria shown in Fig. 7, we compute the growth rate of the vertical instability. The result is plotted in Fig. 8 as a function of the vertical shift, ΔZ. The stabilizing effect of the top wall is quite

evident. In fact, in this particular case, the instability can be suppressed when the plasma-wall distance is less than approximately 3 cm on the top.

Apart from improving the stability of the configuration, the asymmetry has several other effects on the structure of the mode. In Figure 9 (B), we show the ratio between the vertical displacements on the bottom and on the top of the plasma as a function of ΔZ. We note that this ratio, which is always equal to 1.0 for symmetric cases, increases as the plasma approaches the top wall. In addition, the changes in the equilibrium parameters ($\Delta\beta$ and $\Delta\ell$) become important for asymmetric configurations, whereas they are negligibly small in the symmetric case (Fig. 9 (A) and (C)). The effect of asymmetry on the mode structure can also be seen in Fig. 10, where we show the original and displaced flux surfaces for the two extreme cases ($\Delta Z = 0$ and $\Delta Z = 0.34$ m). It should be noted that the displacements shown here are 30 times larger than those used in the calculation of the growth rates.

4. CONCLUSION

It has been shown that a free-boundary equilibrium code can be used successfully to study the positional stability of tokamak plasma with noncircular cross-section. Growth rates of the vertical instability have been computed for a race-track shaped plasma ($b/a = 3$) in a conducting shell with rectangular cross-section. The results obtained for up-down symmetric configurations agree with ERATO calculations. Assuming several different shell heights, the maximum

shell width for stability has been computed. It is shown that current peaking has a very strong destabilizing effect, whereas plasma pressure has practically no influence on the growth rates. Finally, considering the case where the shell is much taller than the plasma, the improvement in stability resulting from an upward shift of the plasma within the shell has been computed. In the case of strong up-down asymmetry, the "vertical displacement" mode also involves changes in shape, beta and current profile.

5. ACKNOWLEDGEMENTS

This work was partly supported by the Swiss National Science Foundation.

References

BERGER D. et al. (1977) Proc. 8th European Conference on Contr. Fusion and Plasma Physics, Prague 1977, Vol. I, p. 52.

BOBBIO S. et al. (1983) Proc. 11th European Conference on Contr. Fusion and Plasma Physics, Aachen 1983, Vol. 7D, Part II, p. 539.

DOBROTT D. et al. (1981) Nucl. Fusion 21, 1573.

GOEDBLOED J.P. et al (1972) Nucl. Fusion 12, 649.

GRUBER R. et al. (1981) Computer Phys. Commun. 21, 323.

HAAS F.A. (1975) Nucl. Fusion 15, 407.

HOFMANN F. and JOYE B. (1983), Lausanne Report LRP 219/83.

HOFMANN F. and Marcus F.B. (1984), Lausanne Report LRP 235/84.

JOHNSON J.L. et al. (1976) in Plasma Physics and Controlled Nuclear Fusion Research (Proc. 6th Int. Conf. Berchtesgaden 1976) IAEA, Vienna, Vol. II, p. 395.

OKABAYASHI M. et al. (1984) in Plasma Physics and Contr. Nuclear Fusion Research (Proc. 10th Int. Conf. London 1984) IAEA Vienna, Vol. I, p. 229.

STAMBAUGH R.D. et al. (1984) ibid., Vol. I, p. 217.

SYKES A. et al (1983(Proc. 11th European Conforence on Contr. Fusion and Plasma Physcis, Aachen 1983, Vol. 7D, Part II, p. 363.

TROYON F. et al. (1984) Plasma Physics and Contr. Fusion 26, 1A, 209.

Figure Captions

Fig. 1: $\Psi = \Psi_{lim}$ surfaces of the original (solid line) and displaced (dashed line) equilibria.

Fig. 2: Racetrack-shaped free-boundary equilibrium with b/a = 3, $\beta = 0.3$, $\ell = -0.5$. The dotted line is the plasma-vacuum boundary.

Fig. 3: Normalized growth rate (Ω^2) vs. shell width (a_w) for various shell heights (b_w). Comparison between ERATO and FBT results.

Fig. 4: Ratio of the vertical displacements on the magnetic axis (H_o) and on the stop edge (H_1) vs. shell width (a_w) for various shell heights (b_w). Comparison between ERATO and FBT results.

Fig. 5: Normalized growth rate (Ω^2) vs. shell width (a_w) for various shell heights (b_w) and for two different values of β.

Fig. 6: Normalized growth rate (Ω^2) vs. shell width (a_w) for various current profiles. Radial current density profiles on the midplane (Z = 0) are shown in the insert.

Figure captions: (cont'd)

Fig. 7: Up-down asymmetric equilibria. ΔZ is the vertical distance between the magnetic axis and the midplane of the conducting shell. Radial profiles of current density and plasma pressure at the height of the magnetic axis are also shown.

Fig. 8: Normalized growth rate (Ω^2) vs. asymmetry parameter ΔZ (= vertical distance between magnetic axis and shell midplane).

Fig. 9: (A) Normalized beta change, (B) stretching parameter H_2/H_1 and (C) current profile change $\Delta\ell$, as a function of the asymmetry parameter ΔZ.

Fig. 10: Flux surfaces of the original (solid line with dots) and displaced (solid line without dots) equilibria for the two extreme cases: $\Delta Z = 0$ (A) and $\Delta Z = 0.34$ m (B). All displacements have been enlarged by a factor 30.

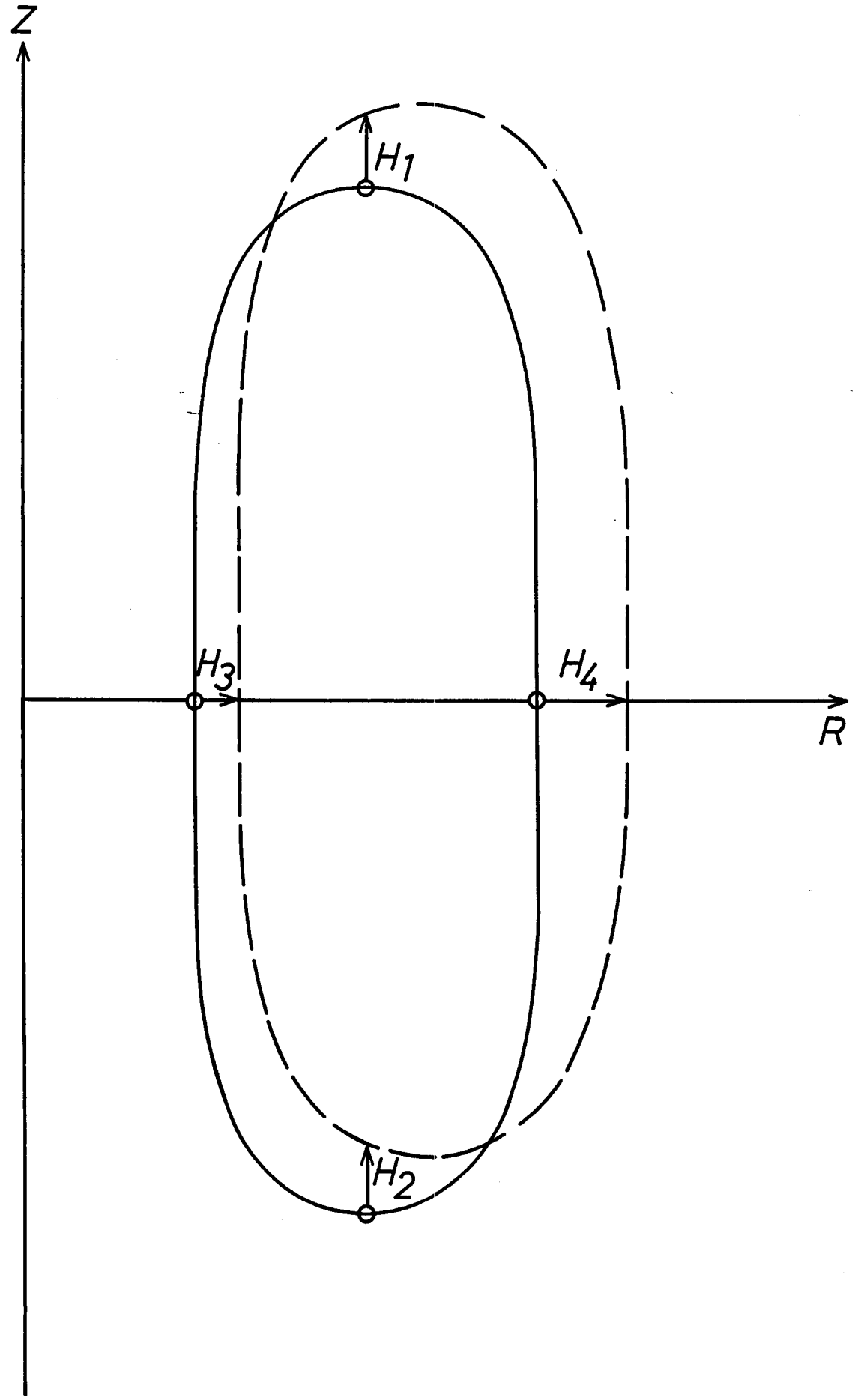

FIG.1

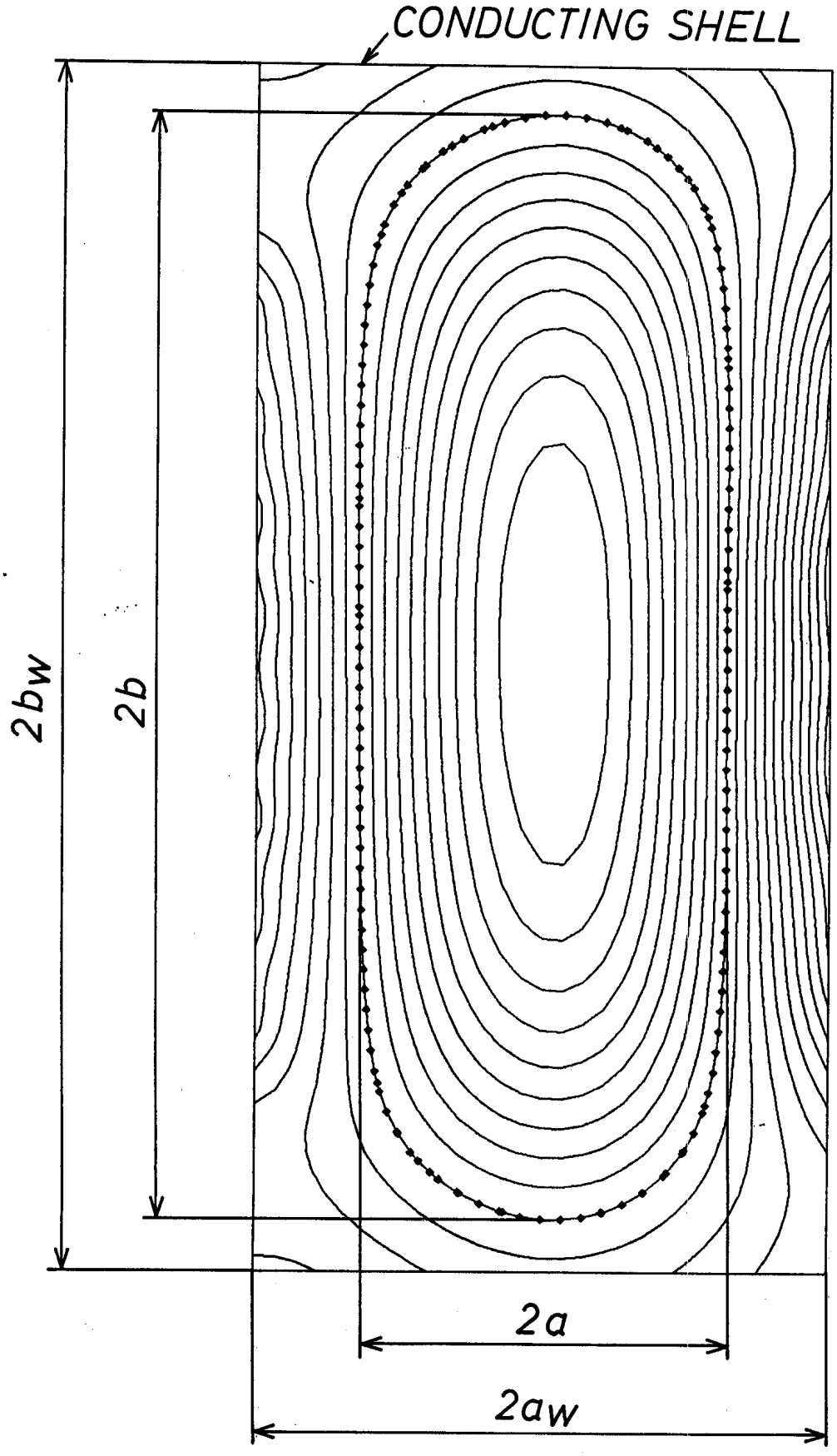

FIG. 2

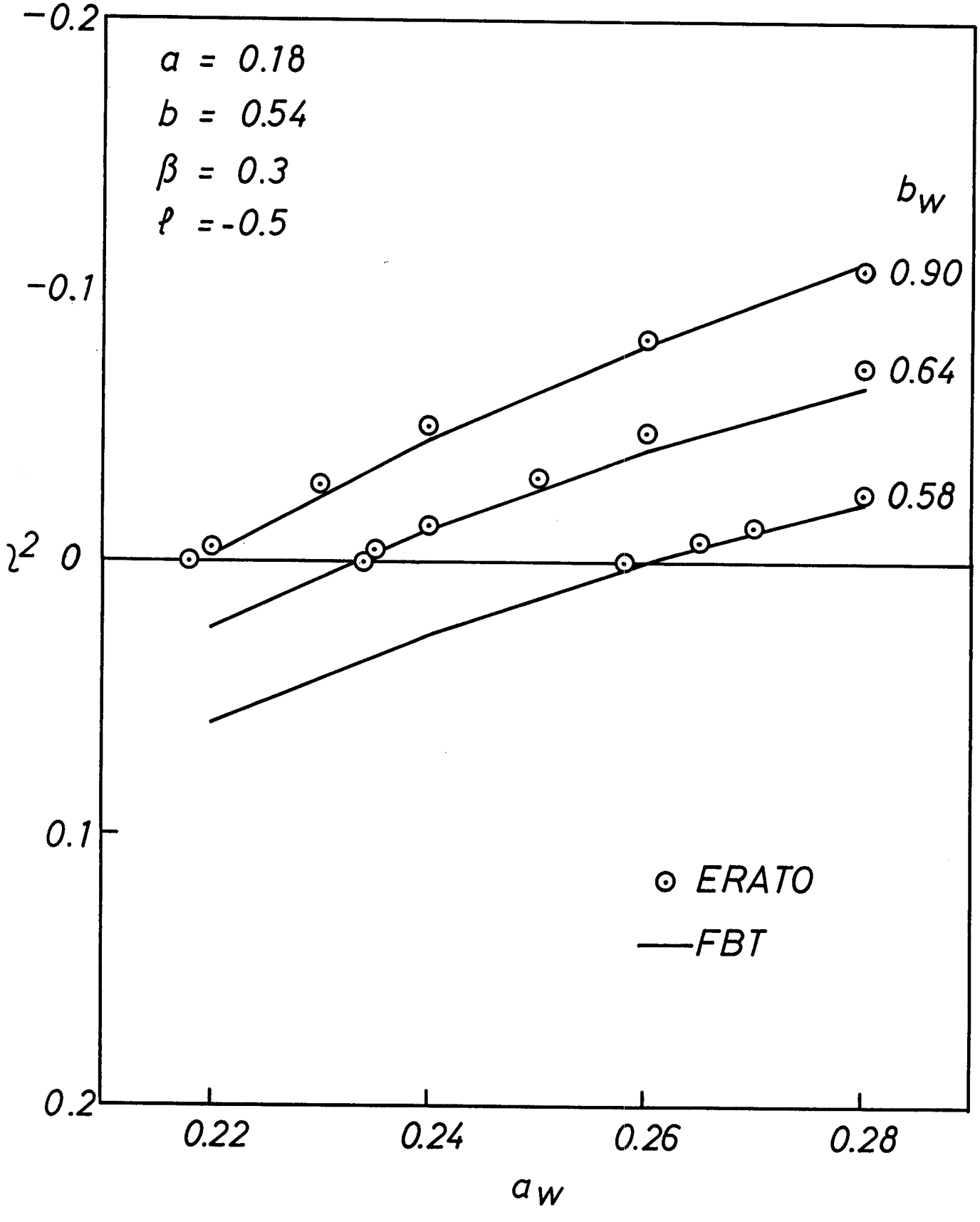
a = 0.18
b = 0.54
β = 0.3
ℓ = -0.5
b_w
0.90
0.64
0.58
-0.2
-0.1
λ^2 0
0.1
0.2
0.22
0.24
0.26
0.28
a_w
ERATO
FBT

FIG. 3

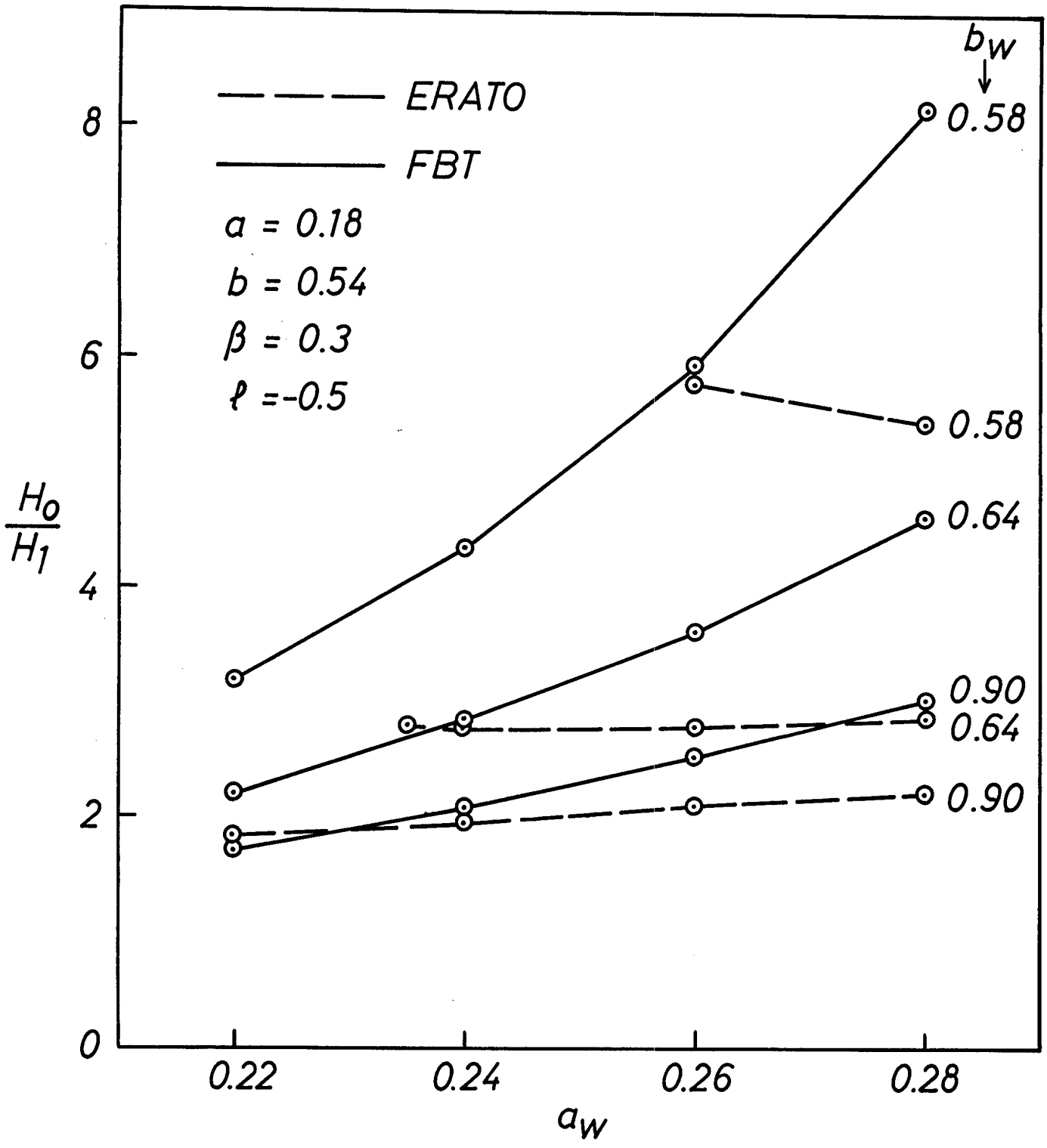
ERATO
FBT
a = 0.18
b = 0.54
β = 0.3
ℓ =-0.5
b_W
0.58
0.58
0.64
0.90
0.64
0.90
$\frac{H_0}{H_1}$
0
2
4
6
8
0.22
0.24
0.26
0.28
a_W

FIG.4

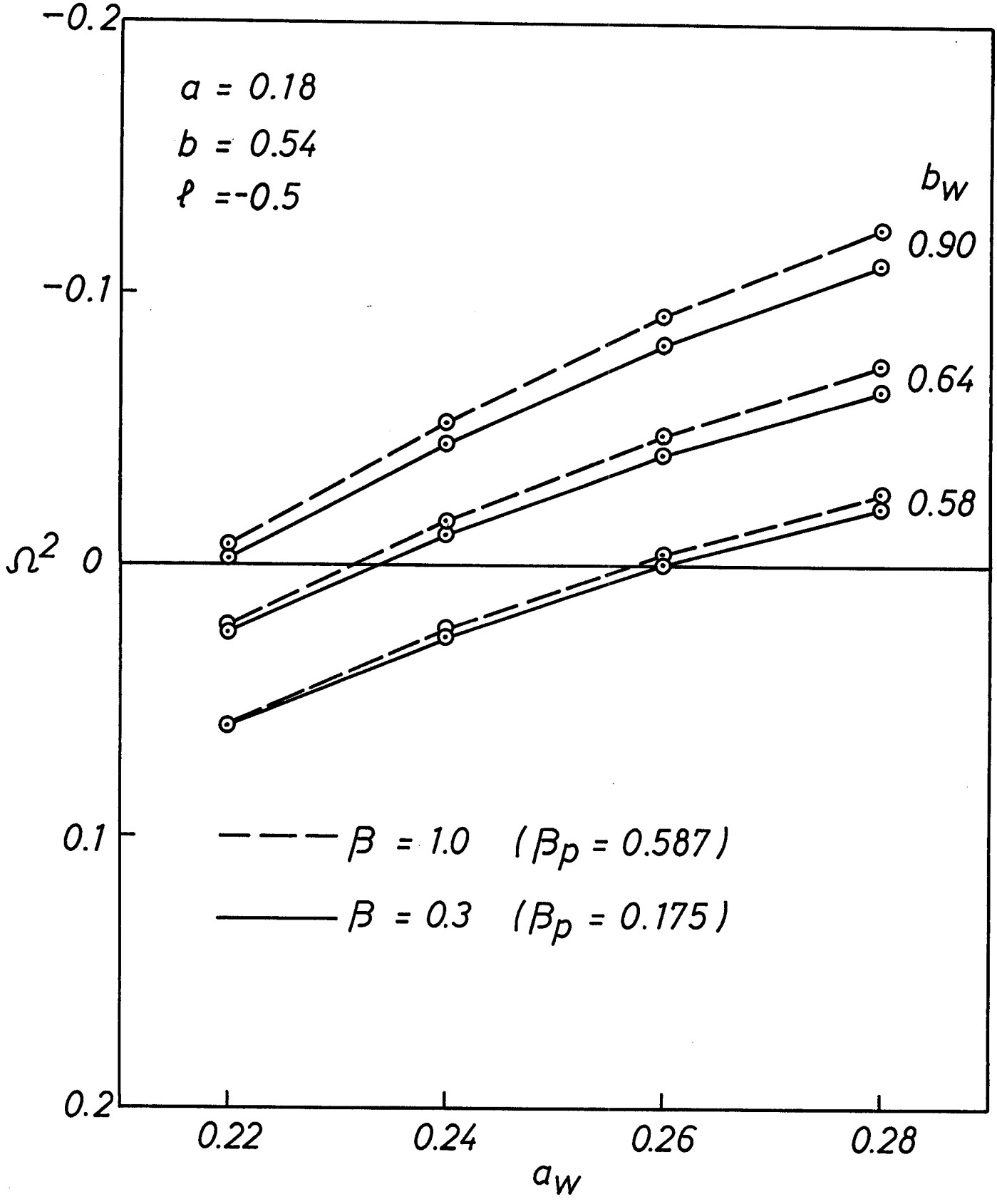
-0.2
-0.1
0.1
0.2
Ω^2 0
a = 0.18
b = 0.54
ℓ =-0.5
b_w
0.90
0.64
0.58
β = 1.0 (β_p = 0.587)
β = 0.3 (β_p = 0.175)
0.22
0.24
0.26
0.28
a_w

FIG. 5

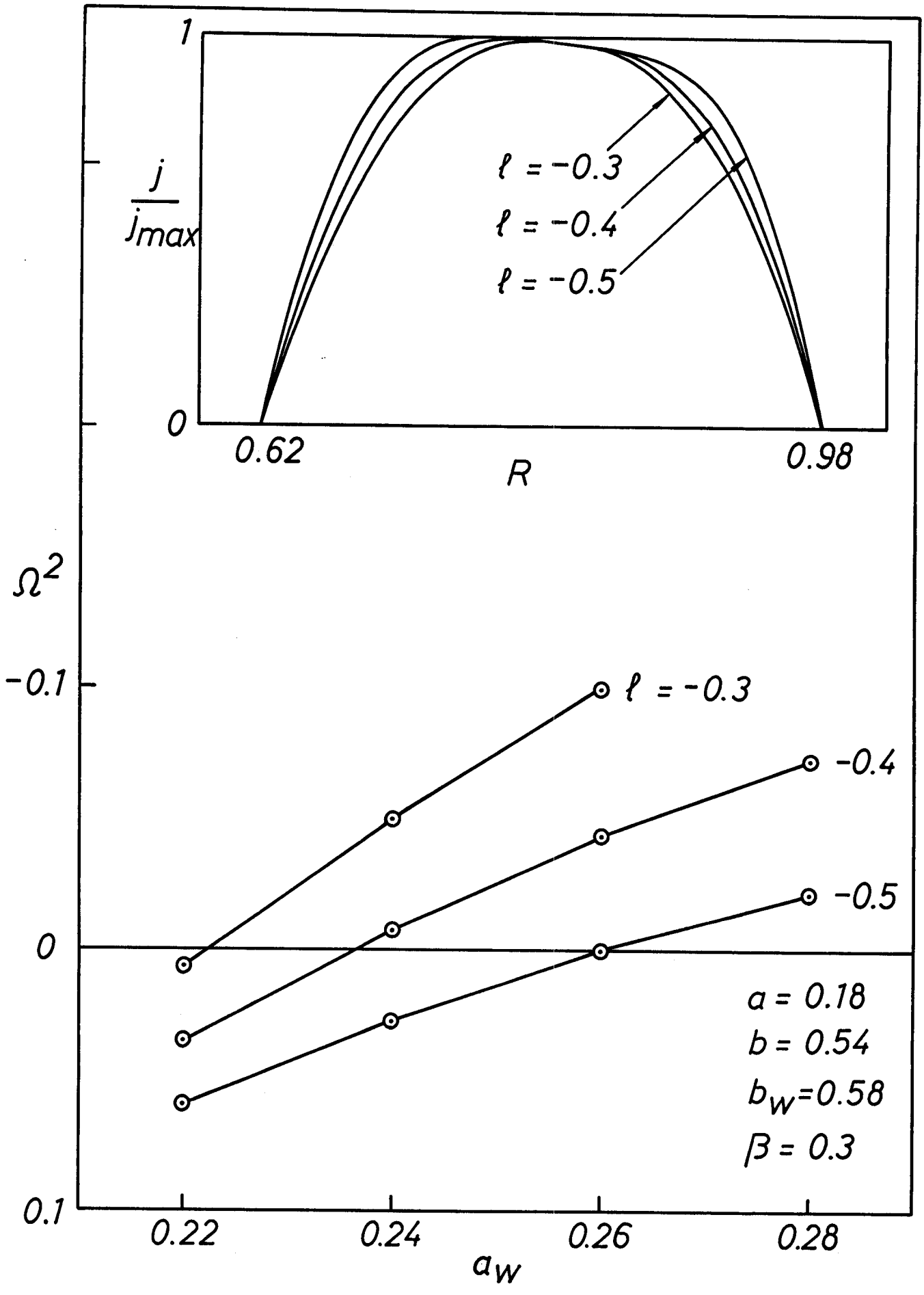
1
j/jmax
0
0.62
R
0.98
ℓ = -0.3
ℓ = -0.4
ℓ = -0.5
Ω²
-0.1
0
0.1
ℓ = -0.3
-0.4
-0.5
a = 0.18
b = 0.54
bW=0.58
β = 0.3
0.22
0.24
0.26
0.28
aW

FIG. 6

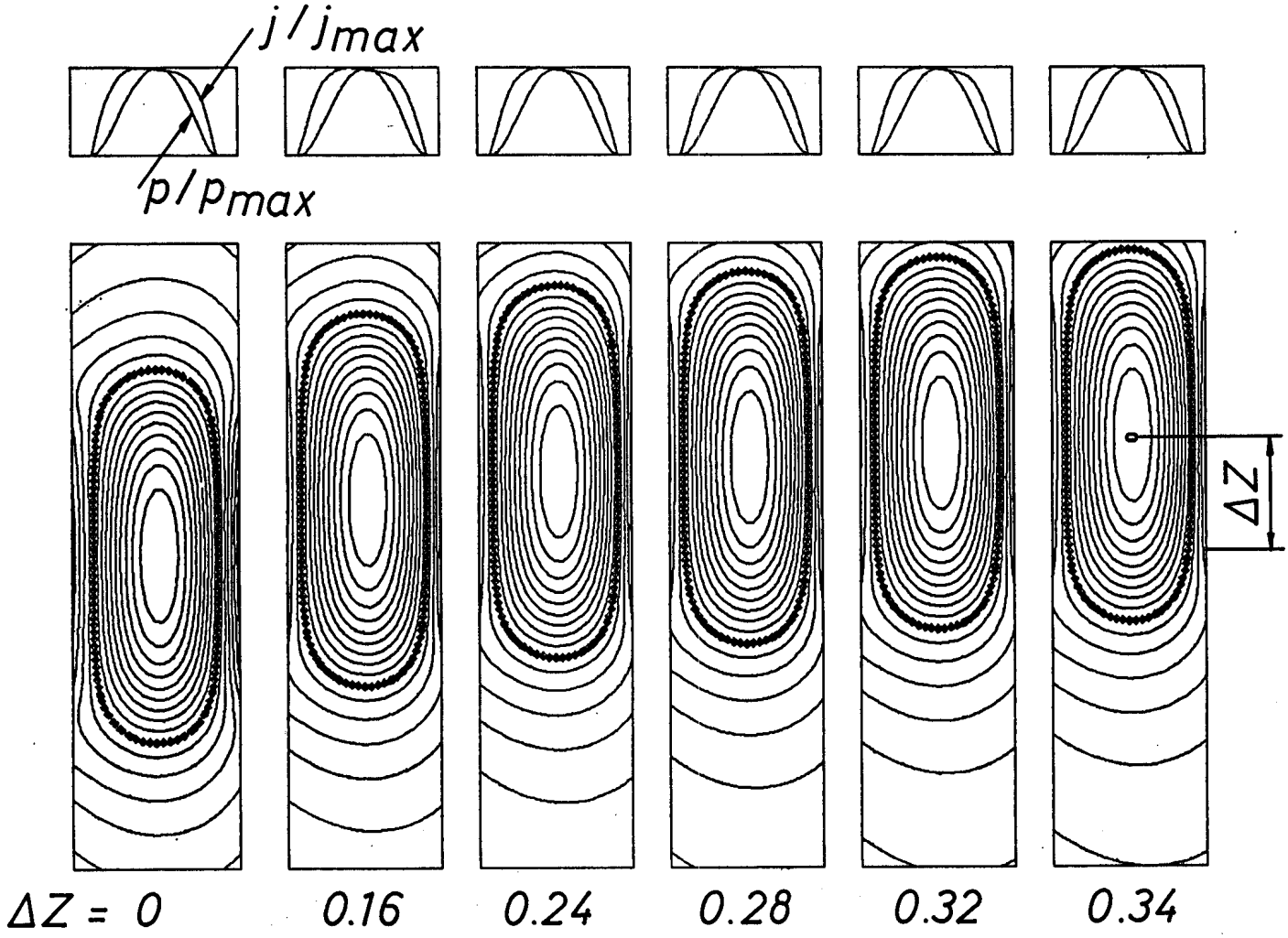

FIG. 7

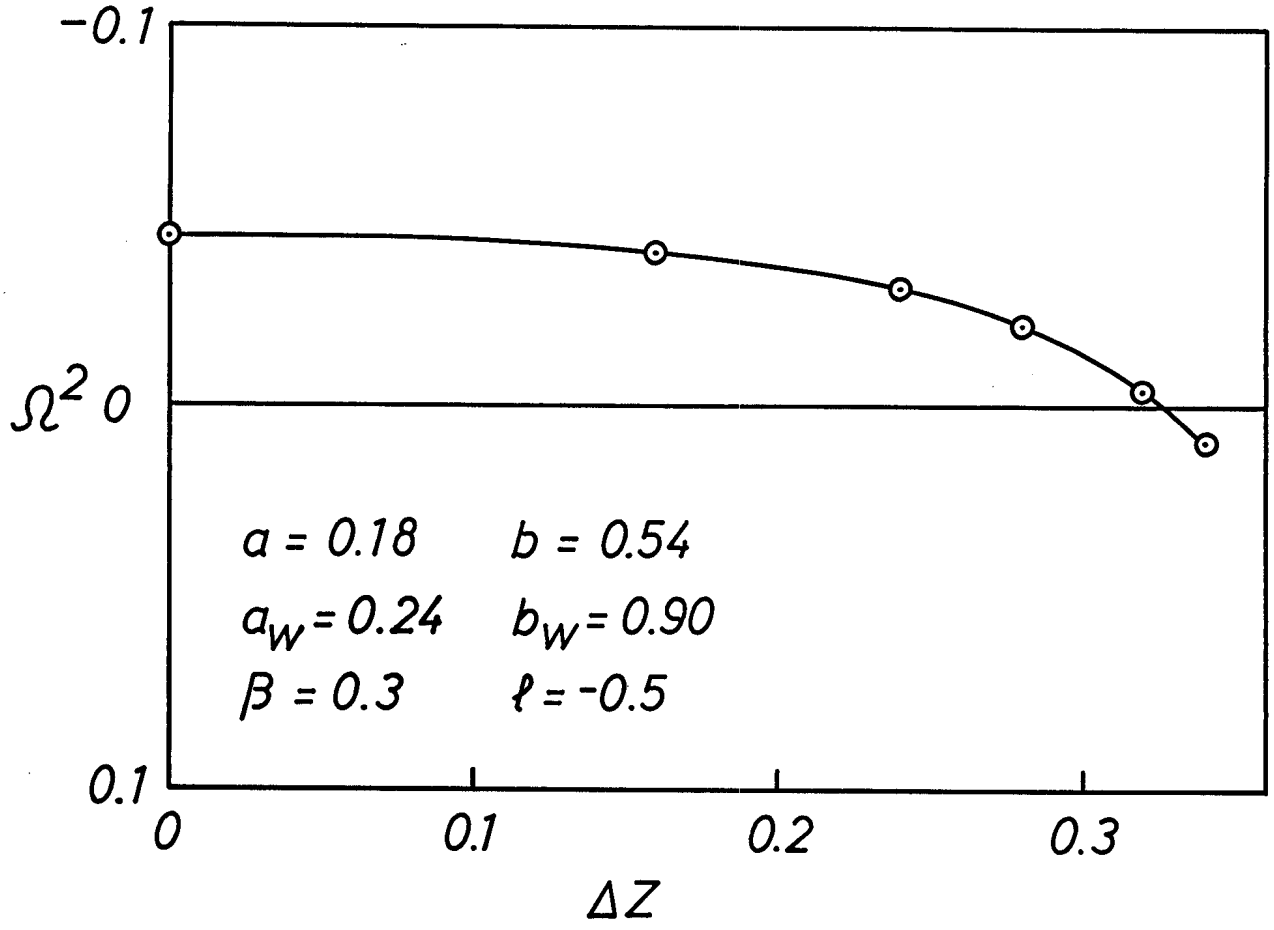
-0.1
$\Omega^2 0$
0.1
0
0.1
0.2
0.3
ΔZ
$a = 0.18$ $b = 0.54$
$a_W = 0.24$ $b_W = 0.90$
$\beta = 0.3$ $\ell = -0.5$

FIG. 8

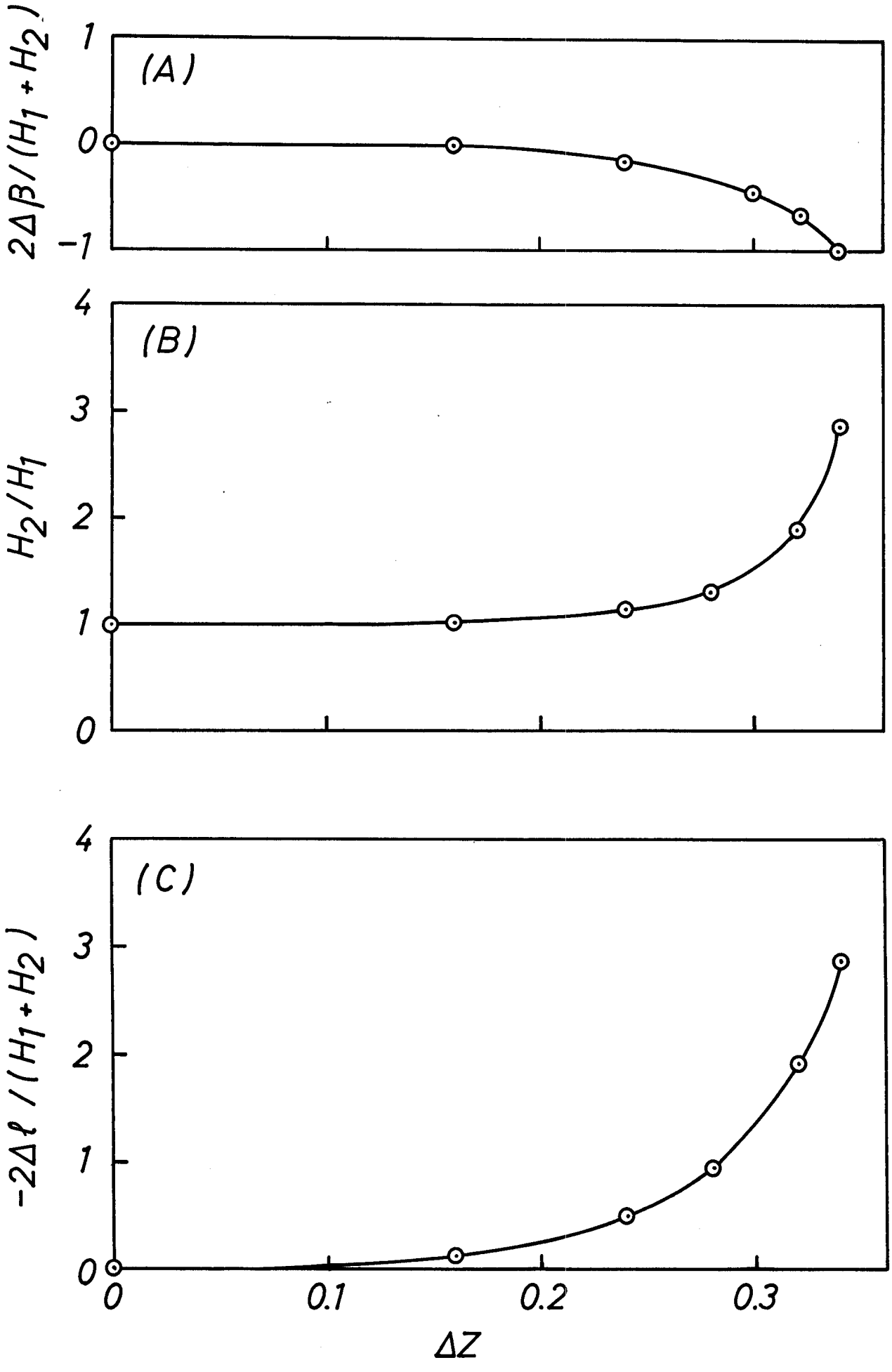
(A)
$2\Delta B/(H_1+H_2)$
1
0
-1
(B)
H_2/H_1
4
3
2
1
0
(C)
$-2\Delta\ell/(H_1+H_2)$
4
3
2
1
0
0
0.1
0.2
0.3
ΔZ

FIG. 9

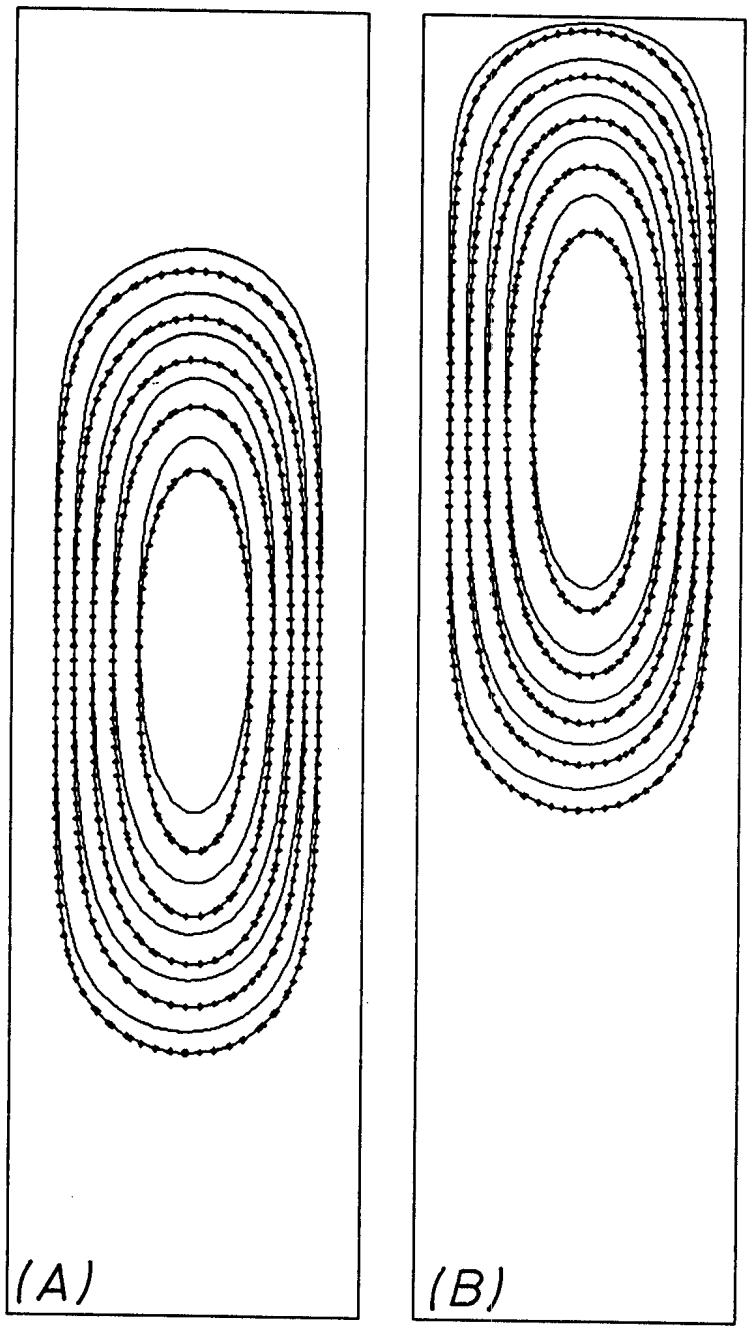

FIG. 10